Fine-time energetic electron behavior observed by Cluster/RAPID in the magnetotail associated with X-line formation and subsequent current disruption

I. I. Vogiatzis, T. A. Fritz, Q.-G. Zong, D. N. Baker, E. T. Sarris, P. W. Daly

Annales Geophysicae, 23, 2265–2280, 2005
SRef-ID: 1432-0576/ag/2005-23-2265

Annales Geophysicae

Fine-time energetic electron behavior observed by Cluster/RAPID in the magnetotail associated with X-line formation and subsequent current disruption

I. I. Vogiatzis[1,2], **T. A. Fritz**[1], **Q.-G. Zong**[1], **D. N. Baker**[4], **E. T. Sarris**[2], **and P. W. Daly**[3]

[1]Center for Space Physics, Department of Astronomy, Boston University, Boston, MA, USA
[2]Space Research Laboratory, Dept. of Electrical and Computer Engineering, Democritus University of Thrace, Xanthi, Greece
[3]Max-Planck-Institut für Sonnensystemforschung, D-37191, Katlenburg-Lindau, Germany
[4]Laboratory for Atmospheric and Space Physics, University of Colorado, Boulder, CO, USA

Received: 8 September 2004 – Revised: 6 June 2005 – Accepted: 20 June 2005 – Published: 15 September 2005

Abstract. Energetic electrons with 90 deg pitch angle have been observed in the magnetotail at ∼19 R_E near local midnight during the recovery phase of a substorm event on 27 August 2001 (Baker et al., 2002). Based on auroral images Baker et al. (2002) placed the substorm expansion phase between ∼04:06:16 and ∼04:08:19 UT. The electron enhancements perpendicular to the ambient magnetic field occurred while the Cluster spacecraft were on closed field lines in the central plasma sheet approaching the neutral sheet. Magnetic field and energetic particle measurements have been employed from a number of satellites, in order to determine the source and the subsequent appearance of these electrons at the Cluster location. It is found that ∼7.5 min after an X-line formation observed by Cluster (Baker et al., 2002) a current disruption event took place inside geosynchronous orbit and subsequently expanded both in local time and tailward, giving rise to field-aligned currents and the formation of a current wedge. A synthesis of tail reconnection and the cross-tail current disruption scenario is proposed for the substorm global initiation process: When a fast flow with northward magnetic field, produced by magnetic reconnection in the midtail, abruptly decelerates at the inner edge of the plasma sheet, it compresses the plasma populations earthward of the front, altering dynamically the B_z magnetic component in the current sheet. This provides the necessary and sufficient conditions for the kinetic cross-field streaming/current (KCSI/CFCI) instability (Lui et al., 1990, 1991) to initiate. As soon as the ionospheric conductance increases over a threshold level, the auroral electrojet is greatly intensified (see Fig. 2 in Baker et al., 2002), which leads to the formation of the substorm current wedge and dipolarization of the magnetic field. This substorm scenario combines the near-Earth neutral line and the current disruption for the initiation of substorms, at least during steady southward IMF. One can conclude the following: The observations suggest that the anisotropic electron increases observed by Cluster are not related to an acceleration mechanism associated with the X-line formation in the midtail, but rather these particles are generated in the dusk magnetospheric sector due to the longitudinal and tailward expansion of a current disruption region and subsequently observed at the Cluster location with no apparent energy dispersion.

Keywords. Magnetospheric physics (Magnetotail; Plasma convection; Storms and substorms)

Correspondence to: I. I. Vogiatzis
(ivogiatz@ee.duth.gr)

1 Introduction

One of the basic features associated with substorms in the near-Earth magnetotail is the injection of energetic particles and plasma (Baker, 1984). Geosynchronous magnetic field reconfiguration and particle injection which take place at the onset of the substorm expansion phase are phenomena associated with the disruption of the cross-tail current and its diversion into the ionosphere via Birkeland currents, to form the substorm current wedge (McPherron et al., 1973). Despite the fact that ions carry much of the cross-tail current, field-aligned current carriers are found to be energetic or plasma sheet electrons. Kaufmann (1987) has suggested that diversion of only the electron cross-tail current to the ionosphere would be sufficient to initiate tail collapse. Furthermore, Jacquey et al. (1991) suggested that the poleward expansion of the auroral electrojet and of the auroral luminosity reflects the motion of the antisunward propagating disruption front, linked to the ionosphere by energetic electrons.

One physical mechanism which is often invoked to explain the energization of particles during a substorm is the near-Earth neutral line (Baker, 1984). However, observations in the plasma sheet indicate that the near-Earth neutral line rarely, if ever, forms within 9 R_E (Lui, 1979). Processes

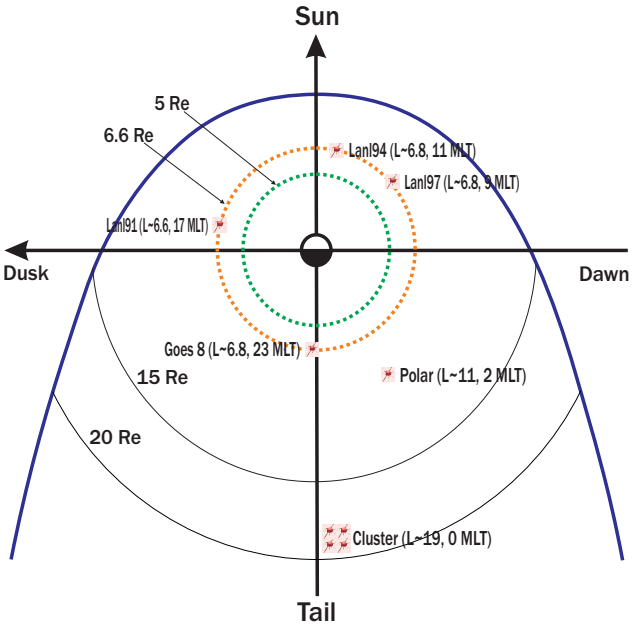

Fig. 1. The average spatial positions of all spacecraft used in this study for the time interval 04:00-04:30 UT.

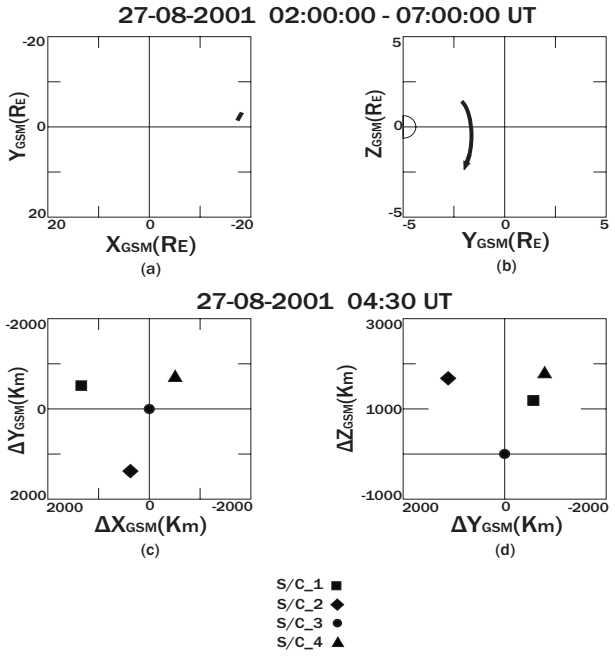

Fig. 2. Cluster trajectory between 02:00 and 07:00 UT in different plane projections, together with the relative position of the four spacecraft in the X–Y and Y–Z planes, in GSM coordinates.

other than X-line formation are responsible for local particle acceleration in the near-Earth magnetotail. Lui et al. (1988) and Lopez et al. (1989) presented observations which are consistent with a turbulent disruption of the cross-tail current sheet. They suggested that the electric fields associated with the turbulent disruption of the cross-tail current are responsible for some of the observed acceleration of energetic particles. Furthermore, current disruption can lead to the release of magnetic stress built up in the near-Earth region during the substorm growth phase, with the result that the highly stretched magnetic field lines are relaxed to become more dipole-like. This magnetic field reconfiguration will undoubtedly energize the particles via Fermi acceleration (shortening of field lines) and betatron acceleration (field magnitude increase as a result of the field collapse). The dipolarization process will also lead to a thickening of the plasma sheet, as indicated by observations (Baker and McPherron, 1990).

In our present paper we address the long standing issue of magnetospheric substorms in the view of our multi-satellite observations and attempt to construct a coherent description of substorm development, in order to explain our Cluster/RAPID energetic particle measurements. Previous works have studied the occurrence and possible energization of energetic particles in the Earth's magnetotail ($X \leq -30\ R_E$), in association with magnetospheric substorms (Sarris and Axford, 1979; Zong et al., 1997, 1998, 2004). These studies attributed the production of high energy particles to the energy dissipated resistively in the reconnection process. However, based on our observations, we conclude that a current disruption/particle acceleration region, expanding both longitudinally and tailward, well after the formation of an X-line deeper in the magnetotail, can account for the generation of the energetic electron event under study and for the appearance, in general, of energetic particles in the midtail.

2 Observations

This study is based on data acquired from the IES (Imaging Electron Spectrometer) sensor system which consists of 3 heads, each one with a 60° opening angle which is part of the RAPID (Research with Adaptive Particle Imaging Detectors) experiment on board Cluster (Wilken et al., 1997). The IES measures energetic electrons within the energy range 20 keV–400 keV. The spatial resolution is 16 azimuthal sectors by 9 polar look directions, covering the entire unit sphere during one spacecraft spin (4 s). The data presented here were obtained when the RAPID spectrometer was operating in a special mode (burst mode) where the resolution is 0.25 s (1/16 of a spin). The data returned from this mode are used to construct intensity distributions on a mercator projection of the unit sphere, with the plane image area comprising 144 pixels. Also, together with the electrons, proton data of 4-s time resolution are used which are provided by the IIMS (Imaging Ion Mass Spectrometer) sensor system, which measures energetic ions within the energy range 10 keV–1500 keV. The plasma data are obtained from the CIS (Cluster Ion Spectrometer) experiment and are of 4-s time resolution, as well (Reme et al., 1997). The Cluster magnetic field measurements are provided from the FGM (Flux/Gate Magnetometer) instrument (Balogh et al., 1997), with a time

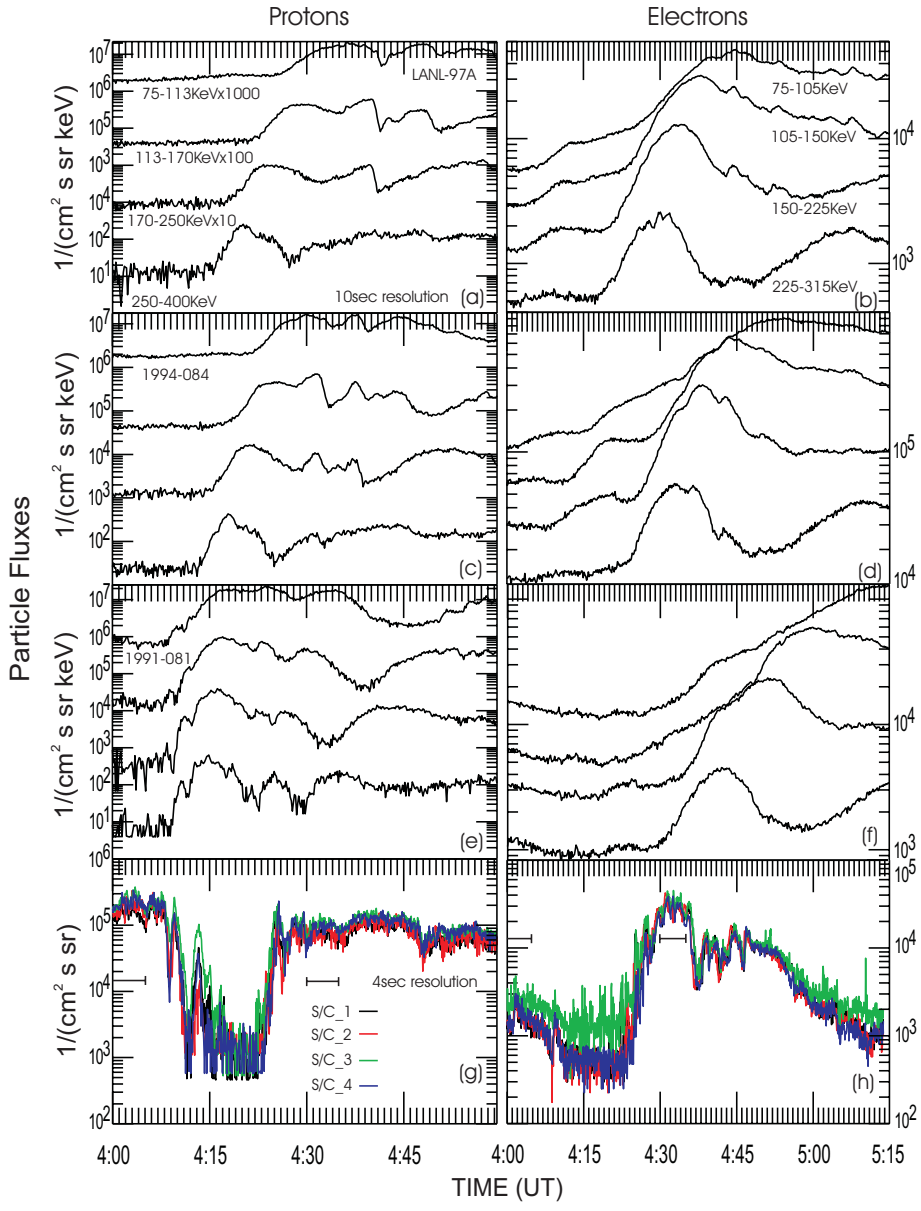

Fig. 3. An overview of proton and electron flux measurements obtained from geosynchronous and Cluster spacecraft between 04:00–05:00 UT and 04:00–05:15 UT, respectively, on 27 August 2001. Also, the horizontal bars denote the time intervals for which the proton and electron energy spectra have been calculated (see Fig. 11).

resolution of 4 s. In addition, concurrent measurements of energetic particle and magnetic field data were used from GOES 8, Polar, and LANL spacecraft, in order to construct a consistent timeline for the particular substorm event.

On 27 August 2001 signatures of a relatively isolated magnetospheric substorm event were observed by a number of Earth-orbiting spacecraft. The average spatial positions of all spacecraft used in this study, for the time interval 04:00–04:30 UT, are shown in Fig. 1. Figure 2 shows the Cluster trajectory between 02:00 and 07:00 UT in different plane projections, together with the relative position of the four spacecraft in the X–Y and Y–Z planes, in Geocentric Solar Magnetospheric (GSM) coordinates. S/C 1, 2, 3, and 4 are marked by a rectangle, diamond, circle, and triangle, respectively. The Cluster constellation was located near apogee (19.2 R_E) around local midnight (00:25 MLT) approaching the equatorial plane from the north, with S/C 3 leading the rest of the satellites on their traverse from the northern to southern lobe.

Figure 3 gives an overview of proton and electron flux measurements obtained from geosynchronous and Cluster spacecraft between 04:00–05:00 UT and 04:00–05:15 UT, respectively, on 27 August 2001. The main features of the plots are centered with respect to the time axes, so that we can have an overall view before and after the principal change in the time profiles. The different panels (a–f) show

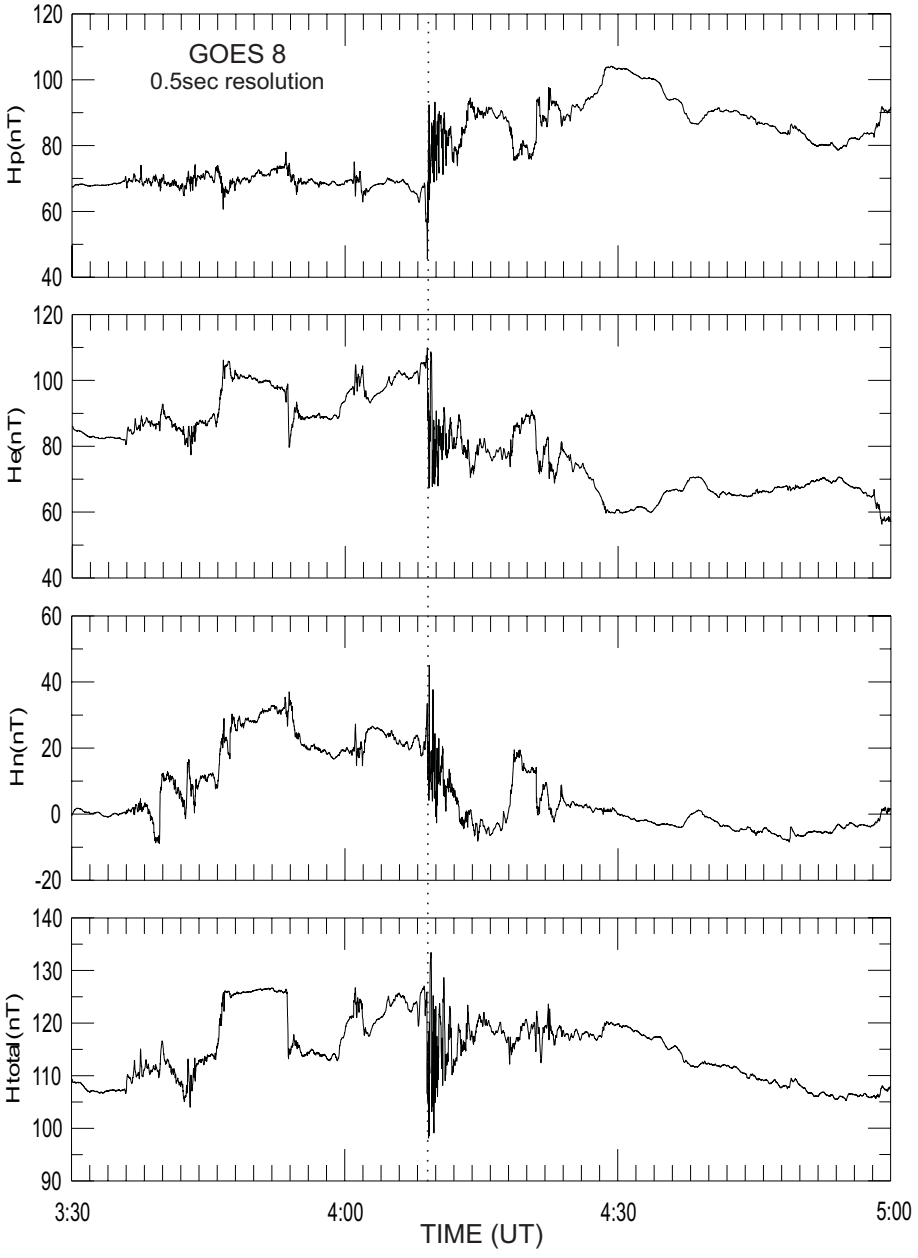

Fig. 4. GOES 8 magnetic field measurements showing a dipolarization onset time at ∼04:09 UT.

differential fluxes of energetic protons and electrons from Los Alamos satellites where there is apparent energy dispersion between the different energy channels. In panels (g) and (h) energy-integrated fluxes are shown from the RAPID experiment. Based on the RAPID/proton data, the Cluster spacecraft were initially inside the plasma sheet, which subsequently appeared to thin, thus letting the satellites enter into a nearly lobe-like environment where the fluxes showed a clear dropout at ∼04:10 UT and then at ∼04:25 UT, the plasma sheet expanded abruptly and re-enveloped all four satellites. An important feature that we want to point out here is that after the plasma sheet expansion the proton fluxes returned to about the same level they had before the dropout, unlike the electron fluxes which showed a clear enhancement during the recovery. Apparently, this happened due to the appearance of a fresh energetic electron population which increased the particle flux levels, where they obtained their maximum value just after 04:30 UT.

Figure 4 gives an 1.5-h interval of GOES 8 magnetic field measurements surrounding the event of interest. The data shown are of 0.5-s time resolution and are presented in the local PEN coordinate system in which the H_p component is parallel to the satellite spin axis, which is perpendicular to the satellite's orbital plane. H_e lies parallel to the satellite-Earth center line and points earthward. H_n is perpendicular to both H_p and H_e, and points eastward. The most obvious

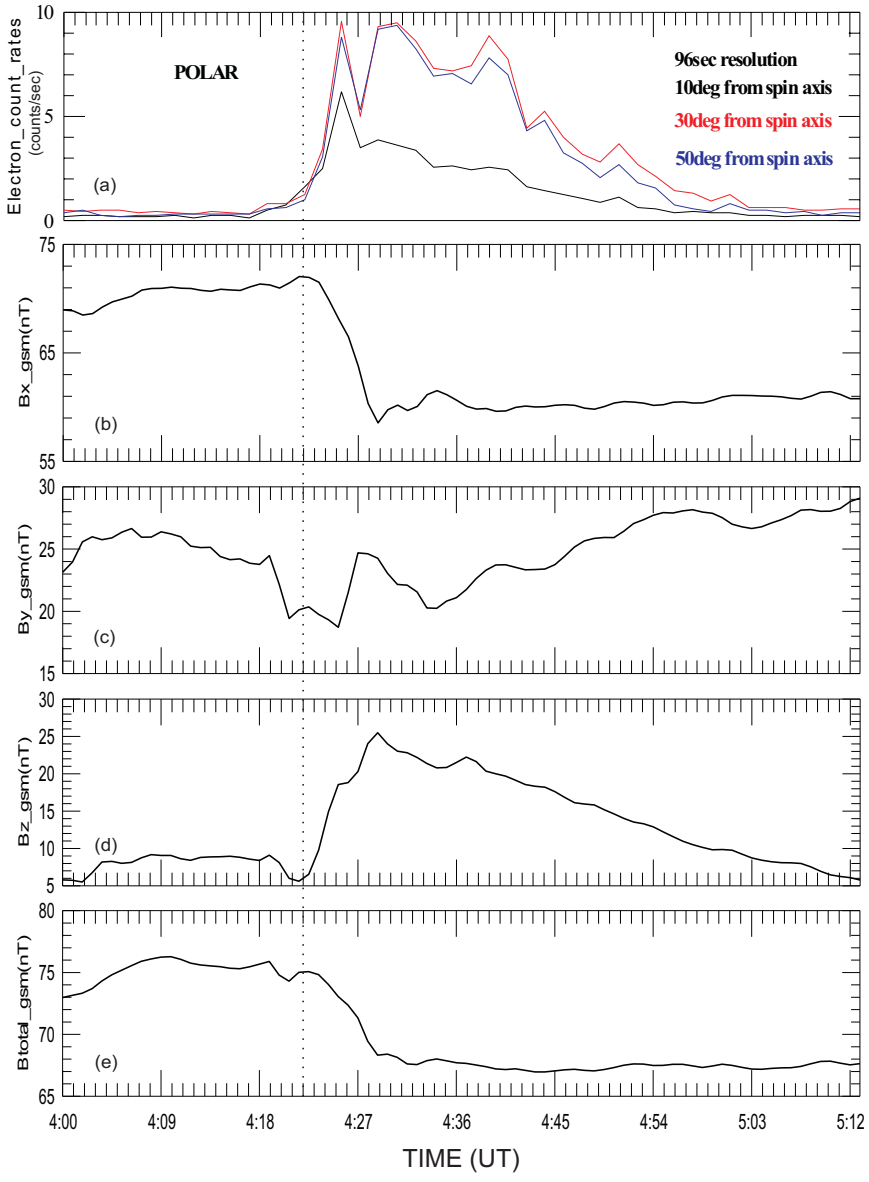

Fig. 5. Electron count rates in three different look directions relative to the Polar spin axis. Also shown are magnetic field components, together with the field magnitude in GSM coordinates. Note the prominent field dipolarization at ∼04:22 UT which coincides with the electron injection.

change in the magnetic field occurred at ∼04:09 UT. Prior to 04:09 UT, the magnetic field had a substantially high magnitude compared to the typical geosynchronous field strength (100 nT) and a relatively stretched configuration, as indicated by the H_p magnetic field component with the elevation angle of the magnetic field vector $\phi = \arctan H_p/H_e$ being around 24 deg. Just at 04:09 UT the field started to become more dipole-like, as revealed by the increasing magnitude of the H_p component accompanied by an interval of ∼2-min duration with strong fluctuations in all the magnetic field components. After the dipolarization onset time the magnetic field magnitude was fluctuating around a mean value and then at ∼04:28 UT started to decrease gradually.

Panel (5a) shows electron count rates from the CEPPAD experiment in the energy range 20 keV–400 keV in three different look directions relative to the satellite spin axis. Panels 5(b)–5(e) show magnetic field components, together with the field magnitude in GSM coordinates. The time resolution is 96 s. The Polar spacecraft at that time was located at L∼11 and 02:00 MLT, as shown schematically in Fig. 1. Its GSM coordinates in Earth radii were (–7.65, –4.47, 3.51), meaning that it was located on the dawn side of the magnetosphere, above the current sheet plane. A main feature that has to be addressed here is the simultaneous enhancement of the electron fluxes in all three different look directions, together with a prominent dipolarization of the magnetic field at ∼04:22 UT. The magnetic field just before the

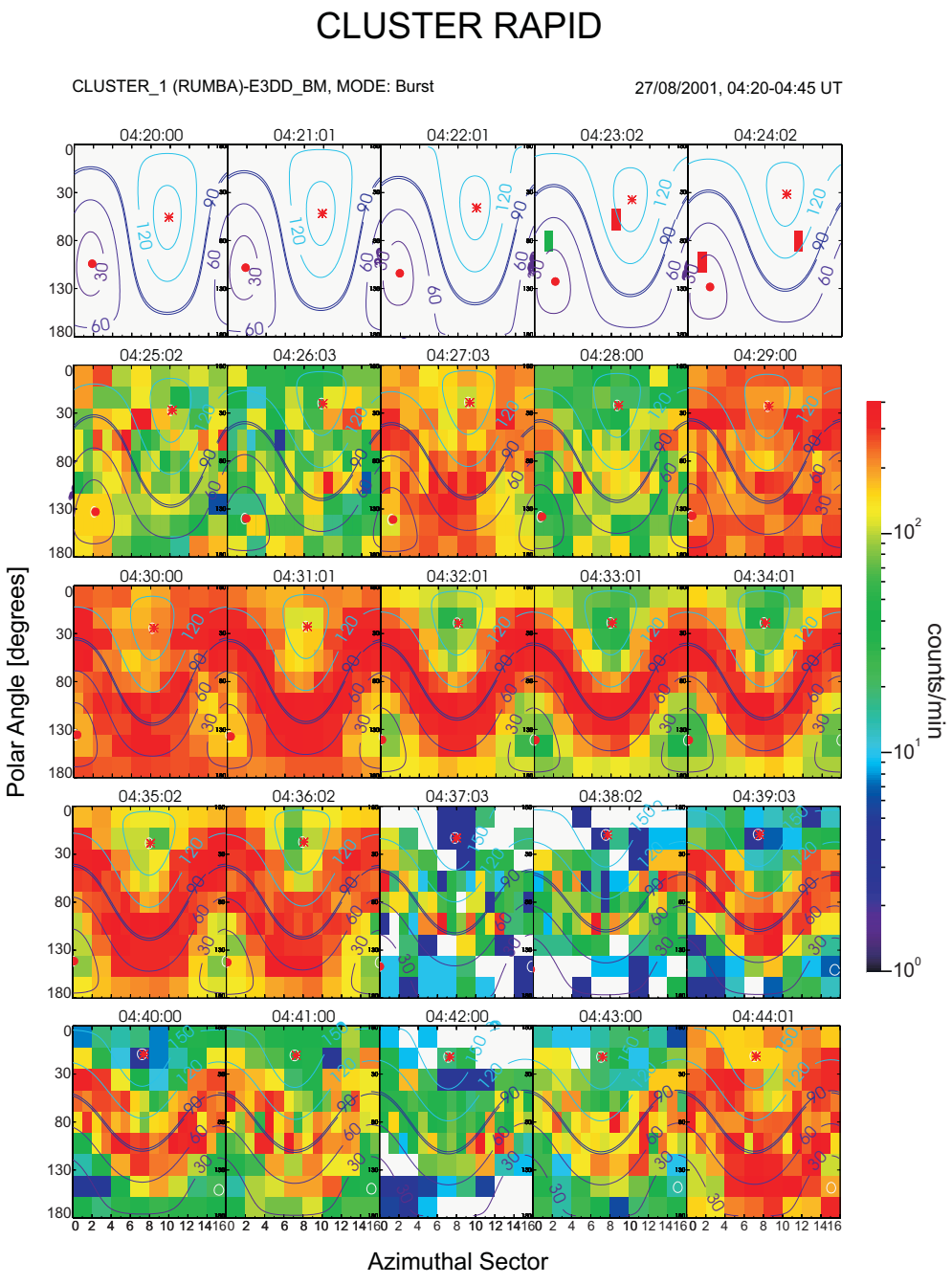

Fig. 6. Representative 3-D intensity distributions from S/C 1. Superimposed are the different pitch angle contours. Note the formation of field-aligned minima at ∼04:30 UT, which last for about 7 min. The dot and the asterisk represent the points where the magnetic field vector intersects the unit sphere.

electron injection was highly stretched, with an elevation angle of the order of 7 deg which reached the maximum value of 24 deg within 7 min, increasing its magnitude by 17 deg.

The strong anisotropic (peaked at 90 deg) electron pitch angle distribution that Cluster observed during its neutral sheet approach is demonstrated in Fig. 6. Here we show representative 3-D intensity distributions from S/C 1, averaged over the first 4 energy channels, over 1 min. The abscissa of each 3-D plane projection corresponds to the 16 azimuthal sectors in which every spin is divided and the 9 polar look directions comprise the ordinate. Superimposed are shown the different pitch angle contours. As is evident we have an abrupt increase in the electron intensity at ∼04:25 UT (plasma sheet expansion), and an isotropic distribution seems to be the dominant feature of this increase, which persists for ∼5 min. At ∼04:30 UT the distribution starts to reveal its anisotropic behaviour by the clear development of field-aligned minima which lasts for about 7 min. After that

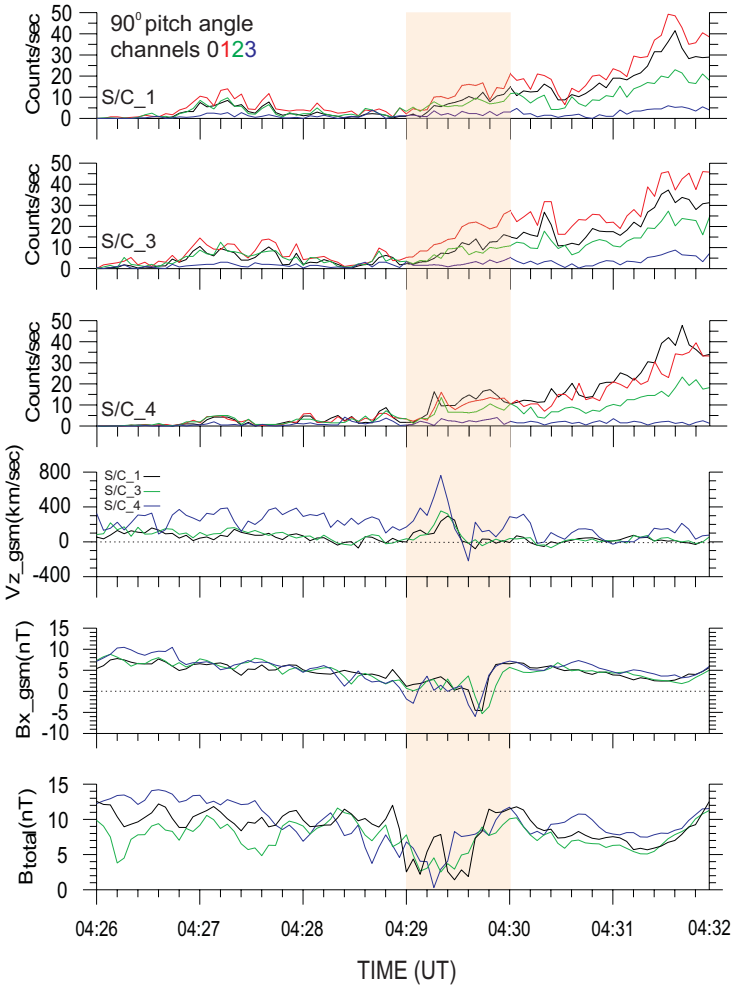

Fig. 7. 4-s time resolution measurements of energetic electron count rates for the first four energy channels and for a 90 deg pitch angle during the beginning of the event. Also shown are the V_z plasma moment, the B_x magnetic field component and the B_{total} magnetic field magnitude.

interval, at ∼04:37 UT, the intensity decreases abruptly but still preserves its anisotropic features. Thus, electrons which are subjected to gradient-curvature drift are traveling dawnward and at ∼04:30 UT make their prominent appearance at the Cluster location.

In Fig. 7 we present in detail the evolution observed by Cluster of the energetic electron intensity enhancements during the period 04:26-04:32 UT for the first four energy channels along with the V_z plasma velocity, B_x magnetic field component and magnetic field magnitude. Note that spacecraft 2 was omitted because the V_z velocity moment was not reliably available at that time. The particle time profiles correspond to electrons traveling perpendicular to the ambient magnetic field, which at that time was in the form of closed field lines (substorm recovery phase (Baker et al., 2002)). While the B_x magnetic field component is close to zero, reversing its sign during the highlighted time interval, the total magnetic field reaches relatively low values, implying that the Cluster fleet was well inside the plasma sheet, very close to the current sheet.

3 Analysis and interpretation

As has been shown in Fig. 3, the substorm event under consideration was accompanied by intense particle injections at geosynchronous altitude. Measurements of energetic particles obtained with a set of three geostationary satellites (LANL-97A, 1994-084, and 1991-081) were used to calculate the longitudinal extension of the substorm injection region. These satellites were located at 09:00, 11:00 and 17:00 MLT, respectively, as shown in Fig. 1. The method to determine the onset times was based on the simple but most reliable, traditional edge detection of selecting onset times by eye, which is also the quickest for a small data set. The method uses the lowest energy channel as a reference to determine the time and inverse-velocity differences with respect to the other energy channels. For each particle species we determine nine points (three for each satellite) and then we calculate the best fit for these points. Typical drift analysis has been performed using expressions which are valid in a dipole field (such as constant drift velocity), and a typical

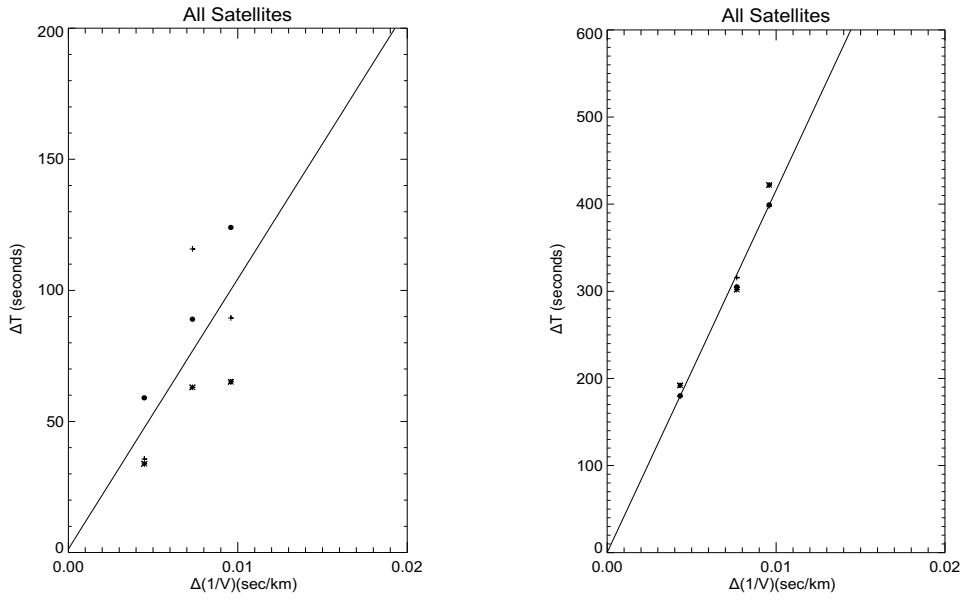

Fig. 8. Determination of the extension of the injection region. It is found to extent from ∼3 deg (relative to dusk meridian toward midnight) to ∼13 deg (relative to dawn meridian toward midnight), with proton and electron injection times at ∼04:09 UT and ∼04:16 UT, respectively. The left panel is for protons, while the right one is for electrons. Also, the plus, the asterisk and the dot signs denote LANL94, LANL97 and LANL91 spacecraft, respectively.

pitch angle of 90 deg was used, which seems to be more appropriate for electrons (Reeves et al., 1990). The results are shown in Fig. 8 (left panel for protons and right panel for electrons), where ideally the lines would go through the (0,0) point. The slopes then determine the location of the outer edges of the combined (proton and electron) injection region with respect to the satellite locations, assuming that the particles of different energies are injected simultaneously. The injection region is then found to extend from ∼3 deg (relative to dusk meridian toward midnight), to ∼13 deg (relative to dawn meridian toward midnight) with proton and electron injection times at ∼04:09 UT and ∼04:16 UT, respectively, having a time lag of ∼7 min, which has also been noted in other cases (Korth et al., 1991; Birn et al., 1997).

At ∼04:06 UT, before the particle injections at geosynchronous altitude, Cluster saw strong earthward plasma flow with B_z being much of the time northward in orientation, as shown in Fig. 9 (first shaded area) (see Baker et al., 2002). After that interval the Cluster spacecraft were intermittently observing high speed earthward flow bursts lasting more than 1 min and exceeding velocities of the order of 700 km/ s, with the magnetic field polarity being positive (second, third and fourth shaded areas in Fig. 9). Such northward reconnected magnetic flux being carried by the fast plasma flows toward the Earth is often considered to be the cause of flux pileup and field dipolarization near the geosynchronous orbit region (Hesse and Birn, 1991). Furthermore, this flux pileup is also regarded as a tailward propagation of a B_z dipolarization signal, often taken as a signal of tailward propagating current disruption (Ohtani et al., 1992).

In combining the observations from GOES 8 and geosynchronous satellites it appears that at 04:09 UT, GOES 8, which was located at 23:00 MLT, made an in-situ observation of the disruption of the cross-tail current associated with a dipolarization of the magnetic field (Takahashi et al., 1987), which, in turn, was directly related to the injection of protons at geosynchronous orbit. These particle observations suggest that the magnetic field reconfiguration/variation was associated with a strong induced electric field ($\partial B_z/\partial t$) that energized the particles (Aggson et al., 1983), an idea that is further supported by Lui et al. (1988).

As already mentioned, based on GOES 8 observations the magnetic field magnitude started to decrease gradually at ∼04:28 UT, something which can be considered to be a "rarefying" dipolarization front propagating tailward, a view that is further supported by Polar observations shown in Fig. 5. Also, based on the fact that the different detector orientations are probing different pitch angle ranges, we may conclude that we do not observe any energy dispersion which otherwise would mean that the particles would have drifted from some point located duskward of the Polar satellite. This transient dispersionless electron burst, together with the reconfiguration of the magnetic field, indicates that a sustained disruption of the local cross-tail current and its diversion into the current wedge has taken place, which, in turn, was remotely sensed by Polar. As we have argued above, at least one particle detector saw field-aligned electrons, meaning that loss cones were filled and current flowed to the ionosphere. One mechanism that can start this process is the onset of a strong particle pitch angle scattering, involving

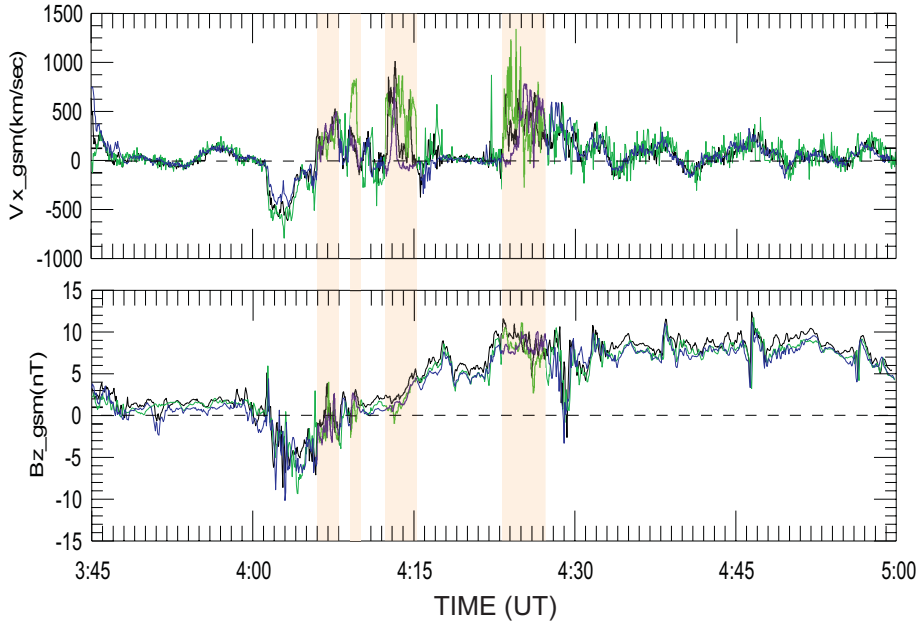

Fig. 9. Intermittent high speed earthward flow bursts exceeding velocities of the order of 700 km/s with northward magnetic field.

wave-particle interactions associated with magnetic turbulence in the neutral sheet, consistent with in-situ observations of current disruption (see Fig. 4). Such scattering fills the particle loss cones and therefore couples the magnetospheric plasma to the ionosphere, thus forming field-aligned currents (FACs). To maintain full loss cones, scattering must be rapid enough, but in this way the electron field-aligned current far exceeds the ion field-aligned current because of the much higher electron velocities. Because the electron current is diverted the field begins to collapse, the ion guiding centers drift less in the more dipolar plasma sheet field, and this reduction in cross-tail current accelerates the collapse (Kaufmann, 1987). By close inspection of Fig. 5c and assuming that the FAC is directed downward, based on the Polar position, we see that the first indication of activity occurs when the substorm current wedge forms on field lines equatorward of the satellite. This produces an eastward perturbation north of the FAC (Nagai, 1982). As the plasma sheet expands (which eventually envelops Polar at ∼04:22 UT (Baker et al., 2002)), the satellite approaches the FAC region. At the edge of the FAC, at ∼04:19 UT, it observes the largest –Y magnetic perturbation (B_y decreases monotonously). As it enters the FAC, at ∼04:20:40 UT, the –Y perturbation diminishes, and as the satellite crosses the center of the FAC region, at ∼04:25:20 UT, the –Y perturbation changes sign (B_y increases monotonously). The above interpretation is consistent with the scenario discussed by Lopez and Lui (1990). Furthermore, the primary contribution to B_{total} before the dipolarization is the addition of the B_x component; thus B_{total} is positively correlated with the cross-tail current, J. Therefore, a disruption/diversion of J will produce a decrease in B_{total}, which seems to be the case (Fig. 5e) (Lopez et al., 1988a). Again, in conjunction with the magnetic field observations at GOES 8, the gradual total magnetic field decrease after 04:22 UT can be viewed in terms of a rarefaction of the total magnetic flux per unit volume, due to the propagation of the dipolarization front tailward with a variable velocity (collapse acceleration).

The global magnetic field reconfiguration is shown in Fig. 10. A schematic 3-D view of the magnetic field lines passing through different satellites is shown, depicting the magnetic field evolution during the event. Just before field dipolarization at ∼04:09 UT, the magnetic field is highly stretched, with relatively small elevation angles (upper panel) while after the dipolarization phase onset and the propagation of the dipolarization front tailward, we start to have the substorm recovery phase. At ∼04:30 UT, when we first start to observe the formation of field-aligned minima, the magnetic field is already relaxed in a more dipolar configuration (lower panel).

By closely examining Fig. 7 we cannot see any observable energy dispersion between the different energy channels in different spacecraft. Assuming that the electrons are subjected to energy-dependent gradient/curvature drift, the above could mean either that we observe the event at its initiation, with the particle source located very close to, and duskward of, the Cluster constellation, or that Cluster intersects the electron drift paths after the event has fully evolved and reached a steady state. One distinct feature in the profiles (shaded area), which favors the second option and facilitates understanding the process, is the gradual increase in the electron intensities that seem to be correlated with large, positive excursions in V_z. These excursions do not show any noticeable time dispersion, which is something that would be expected because of the satellite separations in the z direction. This is due to the fact that the Cluster spacecraft were

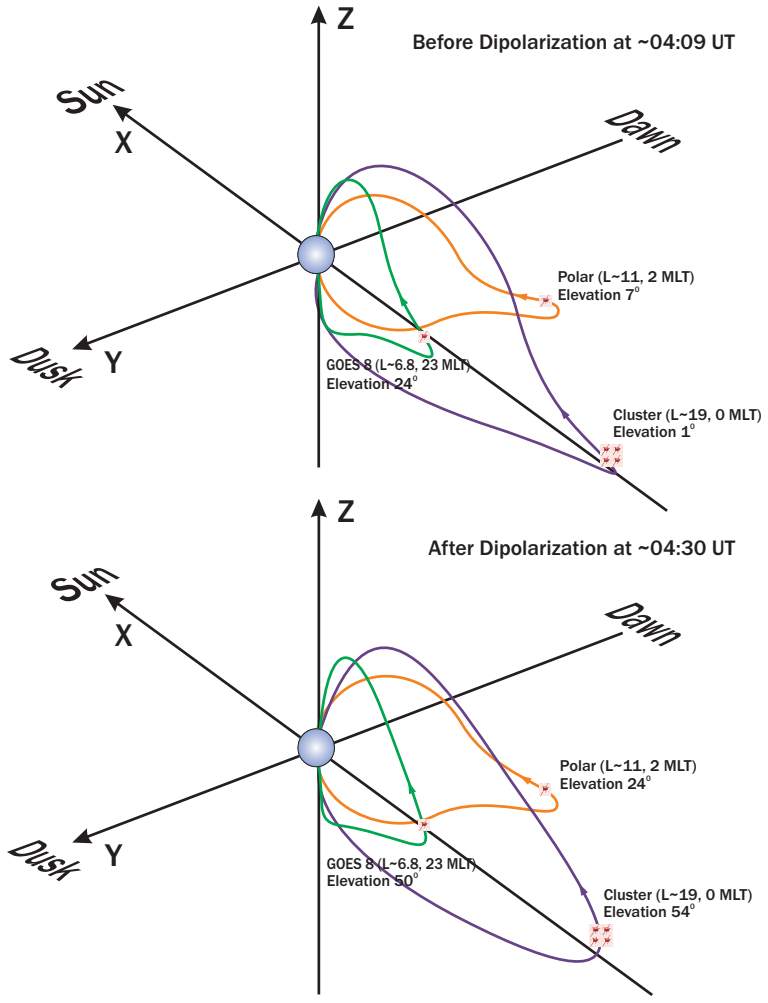

Fig. 10. Global magnetic field reconfiguration during the event. Also shown are the spacecraft positions and the magnetic field elevation angles.

already in the central plasma sheet, so any displacement of the plasma sheet as a whole body resulted in a nearly simultaneous enhancement of the V_z at all spacecraft. Our interpretation (which will be connected with the previous observations) is that the event is already in a steady state, with the drifting electrons generated far duskward of Cluster and being embedded in the center of the dynamical plasma sheet as an independent energetic component. As the latter moves rapidly northward, carrying with it the anisotropic electron population, the Cluster spacecraft eventually intersect the relatively enhanced drifting paths at ~04:30 UT (appearance of field-aligned minima). This happens after the positive excursion in V_z ceases obtaining relatively low values, thus giving the opportunity to observe the intense anisotropic fluxes until 04:37 UT. The latter idea, that the energetic electrons are indeed an independent component of the plasma sheet, is established by examining the energy spectra of protons and electrons shown in Fig. 11. The fact that the proton spectrum remains almost unchanged, even after the plasma sheet expansion at ~04:25 UT, means that we do not have the addition of an extra proton population in the plasma sheet. This is in antithesis with the electrons, where there is obviously the clear softening of the electron spectrum, implying that the fluxes at lower energies owe their existence to the drifting electron population probed by the Cluster constellation, suggesting the spatial nature of the event.

- Estimation of the time and location of the X-line formation

In the following we make an attempt to estimate the time and the position of the X-line formation. We assume that during the initial reconnection the plasma is injected both earthward and tailward, with the same velocity which is taken to be of the order of 500 km/s. This is based on Cluster observations at ~04:01 UT (see Fig. 9), where we have assumed that the tailward plasma velocity between the X-line and the Cluster location remains almost unchanged. Once the earthward flow starts to propagate from the initial reconnection site is subjected to deceleration. Based on auroral images, Baker et al. (2002) concluded that the substorm expansion phase started between ~04:06:16 UT and ~04:08:19 UT. We postulate that the initial earthward flow is fully stopped at

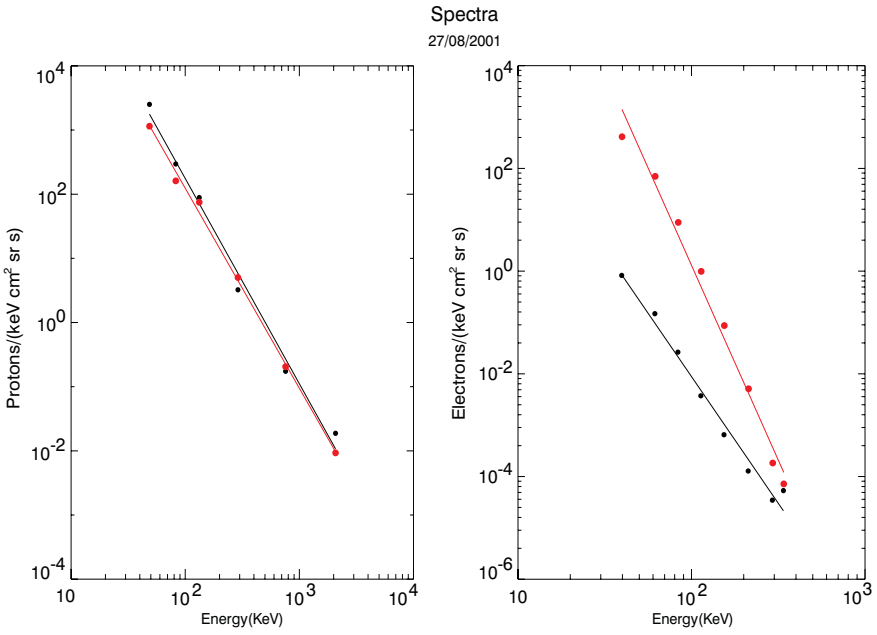

Fig. 11. Representative proton and electron energy spectra from S/C 1 for the intervals 04:00–04:05 UT (black color-coded) and 04:30-04:35 UT (red color-coded) during which the Cluster spacecraft were inside the plasma sheet (see panels (g) and (h) in Fig. 3). Also shown are the calculated best fits for the flux versus energy points. Unlike protons, electrons show a clear softening of their spectrum which is attributed to an additional electron source at lower energies.

∼04:06:16 UT before the time we observe the first dramatic auroral brightening at ∼04:08:19 UT, associated with the beginning of cross-tail current disruption/field dipolarization.

For the calculation of the net deceleration of the initial earthward flow we use the fluid momentum equation for ideal magnetohydrodynamic (MHD) conditions,

$$n_i m_i \frac{d\boldsymbol{v}}{dt} = -\nabla P_T + \frac{1}{\mu_0}(\boldsymbol{B}\cdot\nabla)\boldsymbol{B} \quad (1)$$

For the total earthward pressure gradient we adopt the estimation made by Shiokawa et al. (1997), which is 1.2×10^{-17} Pa/m for a Δx∼8 R_E. For the estimation of the stress term in the right hand-side of Eq. (1) we use magnetic field intensities of B_x∼15 nT and B_z∼2 nT (based on Cluster observations between 03:45–04:00 UT) and a thickness of the tail current sheet where the flows exist at ∼0.5 R_E (Shiokawa et al., 1997). Solving Eq. (1) we find a net deceleration of ∼1.481 km/s^2, where m_i we used the proton mass and n_i a typical ion plasma sheet density of ∼0.4 cm^{-3}.

Combining the above value with the relative times and locations of the (a) initial flow breaking, (b) X-line formation, and (c) tailward plasma flow at the Cluster location, we finally estimate the X-line to have formed at ∼17.5 R_E at ∼04:00:38 UT (see Appendix and Fig. 14 for more details).

The observations described in this study can be combined together to create a consistent event time sequence of the magnetospheric substorm, and of magnetospheric substorms in general, and explain in a satisfactory manner the generation of the unique electron event and its occurrence at the Cluster position. A review of the observations made during the isolated substorm, with which the energetic electron event is intimately associated, is shown in Fig. 12, where a time arrow of the events on 27 August 2001, identified by different satellites is shown. Figure 13 is a schematic illustration depicting our interpretation on how the strong anisotropic electron distribution is produced and subsequently transported toward the Cluster spacecraft. The thick arrows represent the direction of propagation of current disruption. The colored areas represent the expanded regions where particle acceleration has taken place, while the black dashed arrow denotes the path of drifting electrons.

4 Discussion

The Earth's magnetotail is maintained by a current system, which, in the equatorial plane, is directed from dawn to dusk in a sheet whose north-south dimensions are small compared to its extent in the X–Y plane. During the growth phase, this cross-tail current intensifies and moves earthward as the magnetotail becomes more stressed (Kaufmann, 1987). During substorm onset in the near-Earth magnetotail, the stress in the magnetic field is reduced and, as B_x decreases and B_z increases, the field relaxes to a more dipolar configuration. The dipolarization of the magnetic field has been interpreted as a reduction in the near-Earth cross-tail current (Lui, 1978; Kaufmann, 1987). Injections occur simultaneously with the collapse of the tail-like component in the magnetic field, indicating that the occurrence of an injection is simultaneous with the local effects of the diversion of the cross-tail current into the substorm current wedge. We assume that the

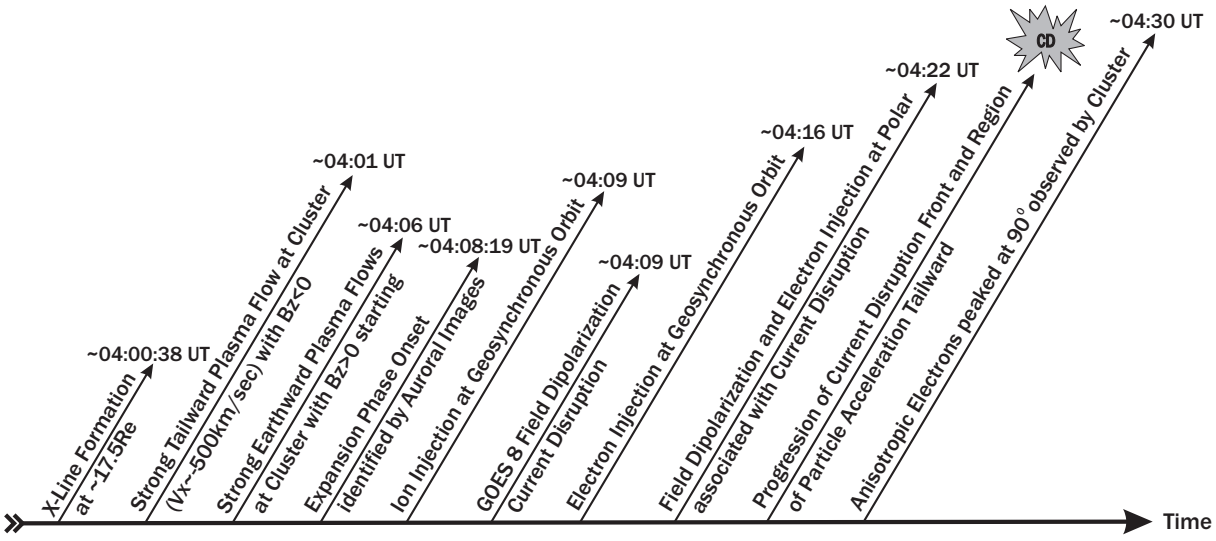

Fig. 12. Review of the observations made during the isolated substorm in the form of a time arrow.

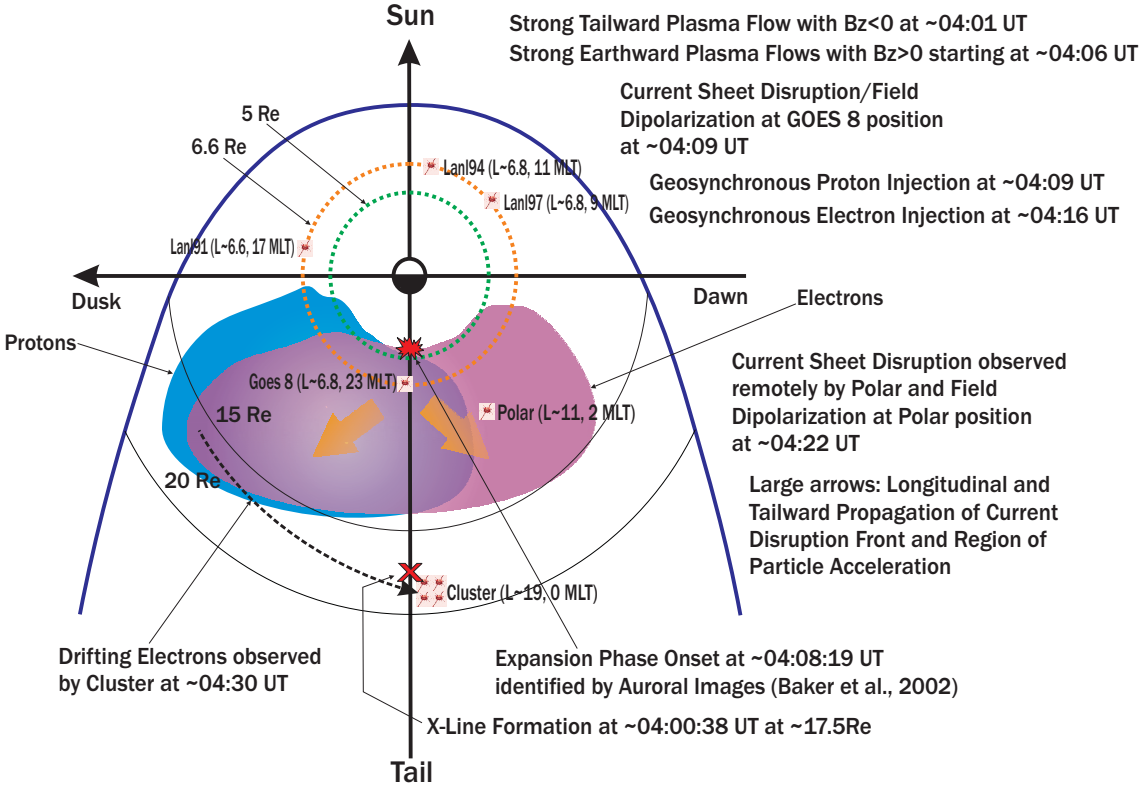

Fig. 13. Qualitative illustration of the scenario on how we envisage the whole process to evolve during the substorm event. We assume that the region affected by the disruption of the cross-tail current expands, both in local time and radius, as the region of instability expands, similar to the way an interface between elastic, crashing bodies propagates backwards with no constant velocity. At the time of expansion phase onset, in a spatially limited region of the cross-tail current sheet near the Earth (which we infer to be inside geosynchronous orbit), the dynamical change in B_z alters the relative drift velocity between ions and electrons, thus triggering in this way an instability (KCSI/CFCI). The excited waves and the associated wave-particle interactions cause particle pitch angle scattering which fills the loss cones diverting the cross-tail current into the ionosphere, thus forming the current wedge. Within the region affected by the disruption, particles are locally energized as the disruption front passes over them. This mechanism is responsible for the energization of the electrons, which are subsequently transported by means of gradient/curvature drift to the Cluster location.

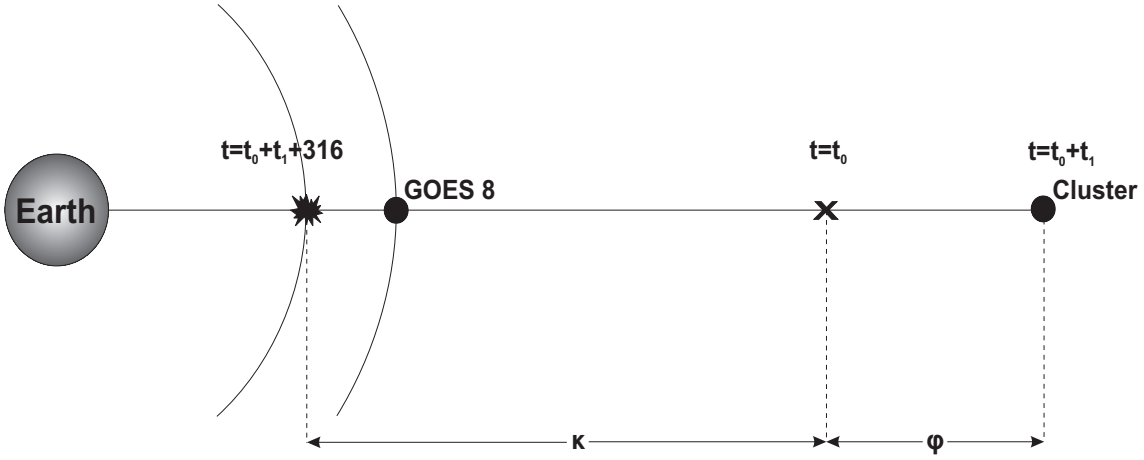

Fig. 14. Schematic diagram illustrating the relative times and distances used in the calculations.

mechanism for the acceleration of energetic particles during substorms in the near-Earth magnetotail is associated with the disruption of the local cross-tail current. This hypothesis explains the correlation between the energetic particle injection and the local magnetic reconfiguration: they are both the result of current sheet disruption. The latter probably results from a local instability, which would explain why the current disruption region has been observed to be azimuthally confined (Nagai, 1982). The most probable onset location in the tail is where the strongest current flows, i.e. where the magnetic field configuration changes from dipolar to tail-like.

Several studies have shown that the local disruption of the cross-tail current expands longitudinally with time, both eastward and westward, from a relatively narrow onset region, which, on average, is at ∼23:00 LT, and that the expansion results in the longitudinal propagation of substorm effects (Nagai, 1982; Lopez et al., 1988b; Lopez and Lui, 1990), with a speed of about 10 km/s to 100 km/s (Arnodly and Moore, 1983). On the other hand, the question of the radial direction of local current disruption propagation has not been definitively answered yet. The prevailing model of earthward propagating injection fronts was first proposed by Russell and McPherron (1973) and was expanded and elaborated on by Moore et al. (1981). However, this model has been questioned based on evidence which indicates that, in some cases, local current disruption was observed to have had a radial component of propagation which was away from the Earth (Lopez et al., 1988b, 1989; Lopez and Lui, 1990; Jacquey et al., 1991). Furthermore, Lui et al. (1988) presented observations of particle intensifications and depletions in very localized ($<1\ R_E$) regions, which argue against the idea suggested by Moore et al. (1981). In addition, the events in that study can be explained by a simple model of current disruption (Lopez et al., 1988a). Based on our study, we further support the latter idea, that local current disruption/particle acceleration not only expands longitudinally and propagates antisunward down the tail, but also begins relatively close to the Earth, inside geosynchronous altitude, which has also been noted before by Friedel et al. (1996), who, based on CRRES satellite data, showed that dispersionless onsets can occur far into the inner magnetosphere, down to L=4.3 and are distributed up to ±5 h around local magnetic midnight.

However, we must point out, as we shall discuss later, that our previous thoughts and the physical view of our study are in complete disagreement with the content of the Li et al. (2003) model. Based on a model which is considering the interaction of an earthward propagating electromagnetic pulse with the preexisting particle populations, Li et al. (2003) succeeded in reproducing the main features shown in panels (a–f) in Fig. 3. In the simulation, the pulse field, which is modeling a dipolarization front propagating toward the Earth, is associated with the recconection which is taking place during the substorm evolution. These simulation results also support the idea of particle acceleration well away from, and earthward of, the actual X-line location.

The neutral sheet stability has been examined by Lui et al. (1990) and Lui et al. (1991), with respect to the kinetic cross-field streaming instability (KCSI) and cross-field current instability (CFCI), respectively. As he pointed out, there are three conditions identified observationally which can trigger a substorm onset: (1) northward turnings of interplanetary magnetic field (IMF) during a southward IMF period, (2) sudden enhancement of solar wind pressure, and (3) steady southward IMF. The condition which applies to our case is the third one, in which a substorm onset is triggered by an internal process during steady southward IMF, which has been reported by Baker et al. (2002). During southward IMF, it is well recognized from observations that both the cross-tail electric field E_y and the B_z component in the neutral sheet, which are the two quantities that determine the amount of ion acceleration in the current sheet region, often exhibit large variations. Numerical solutions to the linear dispersion equations show that the neutral sheet environment is favorable for the onset of the kinetic cross-field streaming/current

instability, which can be a possible trigger for substorm expansions through the generation of oblique whistler waves near the lower hybrid frequency. Both the frequency and the growth rate of this unstable mode become larger by increasing the relative drift speed between ions and electrons. This process can be understood during periods of relatively thin plasma sheet compared to the thermal ion gyro-radius, by invoking the concept of Speiser orbits, where the unmagnetized ions are accelerated by the cross-tail electric field while drifting across the magnetotail (Speiser, 1965). The existence of a magnetic field component perpendicular to the current sheet determines the time that the drifting ions will spend in the current sheet and thus the amount of energy they will gain before they are injected from the current sheet. Consequently, a dynamic change in B_z, due to transportation from a reconnection site (Cluster observations) in the current sheet, changes directly the relative drift speed between ions and electrons, thus providing the necessary and sufficient conditions for the unstable mode to initiate. In this way the excited waves produce magnetic turbulence (GOES 8 observations), while the associated wave-particle interactions fill the loss cones due to pitch-angle diffusion, thus diverting the cross-tail current into the ionosphere through the creation of field-aligned currents (Polar observations).

As we have pointed out at ∼04:10 UT (see panel (g) in Fig. 3), the Cluster spacecraft were embedded in a nearly lobe-like environment until ∼04:25 UT, where the fluxes showed a clear recovery. The first time implies that the tailward edge of the last reconnected closed field line of the detached plasma sheet has passed over the Cluster spacecraft and this, as pointed out by Baker et al. (2002), implies the pinching off of a tailward plasmoid structure before that time. Even after this time point we still observed high-speed earthward flow bursts with B_z positive (third shaded area in Fig. 9), which are attributed to the earthward convection of open (lobe) reconnected field lines. The second time marks the re-entry of the Cluster spacecraft into the plasma sheet/region of closed field lines, which is ascribed to the progression of dipolarization surfaces/region of KCSI/CFCI instability and cross-tail current disruption tailward.

At this point we wish to discuss further the GOES 8 observations. Examining Fig. 4 again, we see that the magnetic field magnitude after the dipolarization onset and before ∼04:28 UT was fluctuating around a mean value. This feature can be attributed to the continuous accumulation of northward B_z in the neutral sheet. On the other hand, the progressively decreasing magnetic field magnitude after ∼04:28 UT implies that GOES 8 started eventually to observe dipolarization surfaces of continuously rarefied magnetic flux per unit volume, propagating tailward. The above can be understood, keeping in mind that a northward magnetic field gives rise to a magnetic pressure acting perpendicular to field lines. Since the plasma is tied to magnetic field lines, it follows that magnetic field lines embedded in an MHD plasma act rather like mutually repulsive elastic bands. Furthermore, the same magnetic field carries a tension along the lines of force, with each flux tube being like an elastic band under tension. With the progression of current disruption/field dipolarization tailward, magnetic pressure prevails against magnetic tension. However, there will be a particular time where magnetic pressure will start to decrease (decreasing magnetic flux per unit volume) and an equilibrium will eventually be achieved when there will be a balance between magnetic tension and magnetic pressure (late stage of substorm recovery phase).

As we have assumed, the initial flow breaking takes place just prior to the cross-tail current disruption, which is manifested by the first dramatic auroral brightening at ∼04:08:19 UT, reported by Baker et al. (2002). From this time on we have a thickening of the plasma sheet progressing backwards, which is facilitated from the reduction of the stress force $(\mathbf{B}\cdot\nabla)\mathbf{B}/\mu_0$ due to cross-tail current disruption/field dipolarization. As we know the total cross-tail current density arising from gradient/curvature drifts and from the gyration effects of the plasma particles is given by

$$\boldsymbol{J} = \boldsymbol{J_d} + \boldsymbol{J_g} = \frac{\boldsymbol{B}}{B^2} \times \left(\nabla P_\perp + \frac{P_\parallel - P_\perp}{B^2} (\boldsymbol{B} \cdot \nabla) \boldsymbol{B} \right) \quad (2)$$

During the reduction of the cross-tail current, we expect that the second term inside the brackets is reduced due to an increase in $P_\perp$ and a decrease in the stress factor. The enhancement of $P_\perp$ will have the effect of significantly changing the plasma distributions, thus producing trapped ("pancake-like") plasma populations along with a magnetic field dipolarization. This is what is indeed observed at geostationary orbit around local midnight (see, for example, the second and third panel in Fig. 1 in Baker and McPherron, 1990).

At this point we would like to emphasize the dual role of the B_z magnetic field component, which is (a) to enhance the northward magnetic flux of the background dipole magnetic field and thus of the magnetic pressure at the transition region between dipolar and tail-like magnetic field configuration, thus increasing in this way the tailward pressure force which decelerates the earthward flows, and (b) to provide the appropriate conditions for the initiation of the KCSI/CFCI instability, which causes the diversion of the cross-tail current and the formation of substorm current wedge. The first role is regarded as the MHD contribution (plasma dynamics) (Shiokawa et al., 1997) to the whole process, which seems to prevail on large spatial and long temporal scales, in antithesis to the second role, which is regarded to be the kinetic contribution (single-particle dynamics) to the whole phenomenon, which takes place in small spatial and short temporal scales. The one does not refute the other, but rather they seem to complement each other.

As we have argued before, the whole phenomenon is evolving in time in the form of an avalanche (collapse acceleration) which can be considered as a self-preserved process that takes place even when there is a lack of high-speed earthward flows with positive B_z in the neutral sheet. This could account for the inconsistency between the duration of the flows and of the substorm current system, as mentioned by Shiokawa et al. (1998). This inconsistency stems exactly

from the fact that the model by Shiokawa et al. (1998) does not take into account the previously mentioned kinetic contribution of the B_z magnetic field component. Yet, the magnetospheric model proposed here applies to the whole substorm expansion phase, unlike the one proposed by Shiokawa et al. (1998), which is limited to only the initial stage of the substorm expansion phase.

In conclusion, we would like to emphasize that some caution is necessary for generalizing the results of the present study, because it is unknown to what extent the features observed in the present event are common. Nevertheless, we do feel that the evolution of the global system, that is cross-tail current disruption triggered by a favorable condition, set up by the reconnection process, is a combination of both phenomena mentioned above with each one having its own importance during the expansion phase of a substorm.

5 Synopsis

We have analyzed a unique electron event observed in the magnetotail at $\sim$19 R_E, closely related to a substorm. In order to end up with a conclusion about the possible mechanism responsible for the generation of these energetic electrons, we have utilized energetic particle and magnetic field observations from a number of spacecraft orbiting around the Earth. We tried to construct a consistent timeline of the events that took place during the substorm ending up with a qualitative substorm onset and development model based on our event related features identified observationally. On the basis of this model we have concluded that the energetic electron measurements made by Cluster are the result of a longitudinal and tailward expansion of current disruption front and region of particle acceleration. This could possibly be the explanatory scenario and for many other similar cases, as well, but it must be noted that is essential events like this one to be explored in a quantitative way in order for the proposed idea explaining the occurrence of the electron population to be substantiated and established.

Finally, the importance of fine-time and angular resolution studies of energetic particles during processes operating in different regimes of the Earth's magnetosphere is an important issue that has been addressed in the present paper. We were able to examine in detail the unique electron event that occurred in the magnetotail based on burst mode data that were available during the time of interest. This special operating mode of the RAPID instrument played a crucial role in constructing the 3-D pitch angle distributions that clearly revealed the strong anisotropic nature of the injected electron population.

Appendix

Expanding the second term in the right hand-side of Eq. (1) and keeping the radial component for which we are interested in, we have

$$\frac{1}{\mu_0}(\boldsymbol{B}\cdot\nabla)\boldsymbol{B} = \frac{1}{\mu_0}\left(\frac{B_x^2}{\Delta x} + \frac{B_x B_z}{\Delta z}\right) \tag{A1}$$

Solving Eq. (1), with the help of the above expansion, we obtain for the deceleration

$$\gamma = \frac{dv}{dt} = 1.481\,\mathrm{km/\,s^2} \tag{A2}$$

where B_x = 15 nT, B_z=2 nT, Δx = 8 R_E = 5096 $\cdot$ 10^4 m, Δz = 0.5 R_E=3185$\cdot 10^3$ m, n_i=0.4$\cdot 10^6$/ m^3, m_i=1.6726$\cdot 10^{-27}$Kg and μ_0=4$\pi\cdot 10^{-7}$N/A^2.

Now let t_1 be the time that passes from the initial X-line formation until the moment Cluster sees the tailward flow at $\sim$04:01 UT. Then, this time satisfies the equation

$$500 - 1.481(t_1 + 316) = 0 \tag{A3}$$

hence,

$$t_1 \approx 22\,\mathrm{s} \tag{A4}$$

For the total distance that the initial flow covers until it stops, we have

$$\kappa = \frac{500\cdot(t_1+316) - (1/2)\cdot 1.481\cdot(t_1+316)^2}{6370} \tag{A5}$$

which gives

$$\kappa \approx 13.2\,\mathrm{R}_E \tag{A6}$$

while the distance that the initial tailward flow covers until it reaches the Cluster location is

$$\varphi = \frac{500 t_1}{6370} \approx 1.7\,\mathrm{R}_E \tag{A7}$$

Thus, the location of the X-line formation from the Earth is estimated to be at 19.2-$\varphi\approx$17.5 R_E, while the corresponding time t_0 is $\sim$04:00:38 UT. Furthermore, the breaking point is estimated to be well inside geosynchronous orbit at 17.5–$\kappa\approx$4.3 R_E.

Acknowledgements. The authors would like to thank the Los Alamos team for providing the geosynchronous energetic particle data and H. Singer for providing the high resolution GOES 8 magnetic field data. I. I. Vogiatzis would also like to thank D. Ntaikos for his assistance in the calculations.

Topical Editor T. Pulkkinen thanks two referees for their help in evaluating this paper.

References

Aggson, T. L., Heppner, J. P., and Maynard, N. C.: Observations of large magnetospheric electric fields during the onset phase of a substorm, J. Geophys. Res., 88, 3981–3990, 1983.

Arnodly, R. L. and Moore, T. E.: The longitudinal structure of substorm injections at synchronous orbit, J. Geophys. Res., 88, 6213–6220, 1983.

Baker, D. N.: Particle and field signatures of substorms in the near magnetotail, in: Magnetic Recconection in Space and Laboratory Plasmas, edited by Hones, E. W., vol. 30, Geophys. Monogr. Ser., 193–202, AGU, Washington D.C., 1984.

Baker, D. N. and McPherron, R. L.: Extreme energetic particle decreases near geostationary orbit: A manifestation of current diversion within the inner plasma sheet, J. Geophys. Res., 95, 6591–6599, 1990.

Baker, D. N., Peterson, W. K., Eriksson, S., et al.: Timing of magnetic reconnection initiation during a global magnetospheric substorm onset, Geophys. Res. Lett., 29, 2190–2193, 2002.

Balogh, A., Dunlop, M. W., Cowley, S. W., et al.: The Cluster magnetic field investigation, Space Sci. Rev., 79, 65–91, 1997.

Birn, J., Thomsen, M. F., Borovsky, J. E., et al.: Characteristic plasma properties during dispersionless substorm injections at geosynchronous orbit, J. Geophys. Res., 102, 2309–2324, 1997.

Friedel, R. H. W., Korth, A., and Kremser, G.: Substorm onsets observed by CRRES: Determination of energetic particle source regions, J. Geophys. Res., 101, 13 137–13 154, 1996.

Hesse, M. and Birn, J.: On dipolarization and its relation to the substorm current wedge, J. Geophys. Res., 96, 19 417–19 426, 1991.

Jacquey, C. J., Sauvaud, J. A., and Dandouras, J.: Location and propagation of the magnetotail current disruption during substorm expansion: Analysis and simulation of an ISEE multi-onset event, Geophys. Res. Lett., 18, 389–392, 1991.

Kaufmann, R. L.: Substorm currents: Growth phase and onset, J. Geophys. Res., 92, 7471–7489, 1987.

Korth, A., Pu, Z. Y., Kremser, G., and Roux, A.: A statistical study of substorm onset conditions at geostationary orbit, in: Magnetospheric Substorms, edited by Kan, J. R. et al., vol. 64, Geophys. Monogr. Ser., 343, AGU, Washington, D.C., 1991.

Li, X., Sarris, T. E., Baker, D. N., and Peterson, W. K.: Simulation of energetic particle injections associated with a substorm on August 27, 2001, Geophys. Res. Lett., 30, 1004–1007, 2003.

Lopez, R. E. and Lui, A. T. Y.: A multisatellite case study of the expansion of a substorm current wedge in the near-Earth magnetotail, J. Geophys. Res., 95, 8009–8017, 1990.

Lopez, R. E., Sibeck, D. G., Lui, A. T. Y., et al.: Substorm variations in the magnitude of the magnetic field: AMPTE/CCE observations, J. Geophys. Res., 93, 14 444–14 452, 1988a.

Lopez, R. E., Baker, D. N., Lui, A. T. Y., et al.: The radial and longitudinal propagation characteristics of substorm injections, Adv. Space Res., 8, (9)91–(9)95, 1988b.

Lopez, R. E., Lui, A. T. Y., Sibeck, D. G., et al.: On the relationship between the energetic particle flux morphology and the change in the magnetic field magnitude during substorms, J. Geophys. Res., 94, 17 105–17 119, 1989.

Lui, A. T. Y.: Estimates of current changes in the geomagnetic tail associated with a substorm, Geophys. Res. Lett., 5, 853–856, 1978.

Lui, A. T. Y.: Observations on plasma sheet dynamics during magnetospheric substorms, in: Dynamics of the Magnetosphere, edited by: Akasofu, S.-I., 563–597, D. Reidel, Hingham, Mass, 1979.

Lui, A. T. Y., Lopez, R. E., Krimigis, S. M., et al.: A case study of magnetotail current sheet disruption and diversion, Geophys. Res. Lett., 15, 721–724, 1988.

Lui, A. T. Y., Mankofsky, A., Chang, C.-L., et al.: A current disruption mechanism in the neutral sheet: A possible trigger for substorm expansions, Geophys. Res. Lett., 17, 745–748, 1990.

Lui, A. T. Y., Chang, C.-L., Mankofsky, A., et al.: A cross-field current instability for substorm expansions, J. Geophys. Res., 96, 11 389–11 401, 1991.

McPherron, R. L., Russell, C. T., and Aubry, M. P.: Satellite studies of magnetospheric substorms on August 15, 1968; 9, Phenomenological model for substorms, J. Geophys. Res., 78, 3131–3149, 1973.

Moore, T. E., Arnoldy, R. L., Feynman, J., and Hardy, D. A.: Propagating substorm injection fronts, J. Geophys. Res., 86, 6713–6726, 1981.

Nagai, T.: Observed magnetic substorm signatures at synchronous altitude, J. Geophys. Res., 87, 4405–4417, 1982.

Ohtani, S., Kokubun, S., and Russell, C. T.: Radial expansion of the tail current disruption during substorms: A new approach to the substorm onset region, J. Geophys. Res., 97, 3129–3136, 1992.

Reeves, G. D., Fritz, T. A., Cayton, T. E., and Belian, R. D.: Multi-satellite measurements of the substorm injection region, Geophys. Res. Lett., 17, 2015–2018, 1990.

Reme, H., Bosqued, J. M., Sauvaud, J. A., et al.: The Cluster ion spectrometry (CIS) experiment, Space Sci. Rev., 79, 303–350, 1997.

Russell, C. T. and McPherron, R. L.: The magnetotail and substorms, Space Sci. Rev., 15, 205–266, 1973.

Sarris, E. T. and Axford, W. I.: Energetic protons near the plasma sheet boundary, Nature, 277, 460–462, 1979.

Shiokawa, K., Baumjohann, W., and Haerendel, G.: Breaking of high-speed flows in the near-Earth tail, Geophys. Res. Lett., 24, 1179–1182, 1997.

Shiokawa, K., Baumjohann, W., Haerendel, G., et al.: High-speed ion flow, substorm current wedge, and multiple Pi 2 pulsations, J. Geophys. Res., 103, 4491–4507, 1998.

Speiser, T. W.: Particle trajectories in model current sheets, J. Geophys. Res., 70, 4219–4226, 1965.

Takahashi, K., Zanetti, L. J., Lopez, R. E., et al.: Disruption of the magnetotail current sheet observed by AMPTE/CCE, Geophys. Res. Lett., 14, 1019–1022, 1987.

Wilken, B., Axford, W. I., Daglis, I., et al.: RAPID: The imaging energetic particle spectrometer on Cluster, Space Sci. Rev., 79, 399–473, 1997.

Zong, Q.-G., Wilken, B., Reeves, G. D., et al.: Geotail observations of energetic ion species and magnetic field in plasmoid-like structures in the course of an isolated substorm event, J. Geophys. Res., 102, 11,409–11,428, 1997.

Zong, Q.-G., Wilken, B., Woch, J., et al.: Energetic oxygen ion bursts in the distant magnetotail as a product of intense substorms: Three case studies, J. Geophys. Res., 103, 20,339–20,363, 1998.

Zong, Q.-G., Fritz, T. A., Pu, Z. Y., et al.: Cluster observations of Earthward flowing plasmoid in the tail, Geophys. Res. Lett., 31, doi:10.1029/2004GL020 692, 2004.